Interlaminar fracture toughness of 5HS C/PEEK laminates. A comparison between DCB, ELS and mandrel peel tests.

Francisco Sacchetti[a,b] Wouter J.B. Grouve[a], Laurent L. Warnet[b], Irene Fernandez Villegas[c]
a *ThermoPlastic Composites Research Center (TPRC), Enschede, The Netherlands*
b *Faculty of Engineering Technology, Chair of Production Technology, University of Twente, Enschede, The Netherlands*
c *Structural Integrity and Composites, Faculty of Aerospace Engineering, Delft University of Technology, Delft, The Netherlands*

Abstract

The present work focuses on the applicability of the mandrel peel test to quantify the interlaminar fracture toughness of 5 harness satin woven fabric carbon/PEEK composites. For this purpose, the Mandrel Peel (MP) test was compared to the Double Cantilever Beam (DCB) and End-Loaded Split (ELS) test in terms of experimental procedure and obtained results. The interlaminar toughness of the 5 harness carbon/PEEK was measured both parallel and perpendicular to the predominant fibre direction at the interface. While stable crack propagation was observed in the ELS test, unstable crack propagation (stick-slip) was observed during both the DCB and the mandrel peel tests. In the case of the mandrel peel test, however, the unstable propagation was immediately arrested by the mandrel, limiting the instability and providing numerous crack re-initiation values per unit of crack length. This effect is expected to increase the statistical relevance of a single test and thereby to increase the reliability of the measured values as compared to DCB tests. A fractographic analysis was performed to study the nature of the crack propagation for the different testing techniques. The mandrel peel test was found to be a potentially plausible alternative to the DCB test for woven fabric reinforced composites.

1. Introduction

Woven fabric composites are sometimes preferred to unidirectional tape materials for their simpler handling and better drapability. Woven fabric composites are also known to be more damage tolerant than their unidirectional counterparts in the presence of a delamination [1]. The higher damage tolerance is often explained by the irregular interlaminar structure of woven fabric composites which forces a delamination (crack) to interact with the matrix regions and the weave structure during the its propagation, leading to a more tortuous crack path [2] [3]. The fracture toughness of woven fabric composites is determined by a number of factors, which include the structure of the weave, referred to as weave index [2] [4] [5], the stacking sequence and the direction of crack propagation [4] [6] [7] [8].

Although interlaminar failure of composite materials is a well-known problem, limited data is available on the toughness of woven fabric reinforced composites. This is partly caused by the difficulty associated with experimental characterization. Various test methodologies, all based on Linear Elastic Fracture Mechanics (LEFM), have been developed for unidirectional fibre reinforced composites. Some of the more accepted ones are the Double Cantilever Beam test (DCB) for mode I, and the End-Loaded Split (ELS) or End Notch Flexure (ENF) for mode II. Figure 1 schematically represents the DCB and ELS tests. The existence of ISO and ASTM standards for both methods, although restricted to unidirectional composites in the longitudinal direction, illustrates some maturity of these testing techniques. While the DCB test for mode I is well accepted, this is not (yet) the case for the ELS and ENF tests for mode II, as the introduction of the standards is relatively new. Besides, both tests suffer from some experimental difficulties such as the inability to accurately measure crack length and the lack of a clear method to account for the friction between the arms of the specimen. Moreover, crack propagation is not always stable which further complicates the analysis. [9, 10].

Mode I - DCB Mode II – ELS Mixed mode – mandrel peel

Figure 1: DCB, ELS, and mandrel peel test scheme

Although standardized for UD laminates, some difficulties arise when the DCB test method is used to characterise woven fabric composite laminates. In particular, woven fabric reinforced

composites often show unstable crack propagation (stick-slip). This is true both for thermoset [2] [6] [7] [8] and thermoplastic [11] [12] [13] composites. The unstable crack propagation yields only a few G_{IC} values per test specimen. Therefore, G_{IC}-unstable propagation values for woven fabric reinforced laminate specimens are statistically less reliable than G_{IC}-stable propagation values for UD specimens [14]. Moreover, the unstable crack propagation makes the interpretation of the test results rather difficult and the comparison with unidirectional materials questionable. The stick-slip behaviour has been treated from a theoretical point of view by different researchers such as in [15], [16], [17], [18], [19]. Hine et al. reported that unstable crack propagation in woven fabric composites is caused by local regions of high toughness [20]. When the cracktip reaches one of these tougher regions, crack propagation is slowed down until the stored elastic energy is sufficient to propagate the crack further. Once this region is passed, the elastic energy stored is higher than required for stable propagation. As a result the crack propagation rate increases, resulting in unstable crack propagation. For woven fabrics, the tougher regions have been correlated to the areas where the crack passes over a transverse fiber bundle [7].

The observed stick-slip behaviour and the tedious test procedure make the DCB test unattractive for woven fabric reinforced composites. The Mandrel Peel (MP) test is investigated as an alternative test to measure the interlaminar fracture toughness of woven fabric thermoplastic composites, in the present work. The mandrel peel test is an adaptation of the standard peel test, which is used to measure the bond strength of an assembly of two adherents where one adherent is flexible and the other is rigid [21]. The adherents are pulled apart at a steady rate in such a way that separation occurs progressively along the length of the bonded adherents. When the peel test is used for tough composite materials the radius of the peel arm near the crack tip becomes too small during the loading phase of the test, resulting in the fracture of the peel arm before crack propagation. The mandrel peel test was first proposed by Kawashita et al. [22], as an adaptation of the peel test, in order to measure the fracture toughness of a metal-epoxy-metal peel specimen. Previous research showed that this test can also be used to characterise the fracture toughness of UD-UD [23] [24], UD-woven [24], and UD-metal [25] interfaces. The peel arm, which was a UD tape in these cases, was forced to conform to a mandrel by using an alignment force. The radius of the mandrel was chosen such that the maximum strain in the peel arm does not exceed its failure strain. It should be noted that the fracture toughness evaluated using the mandrel peel test corresponds to a mixed mode propagation. Although the exact mode mixity is unknown, it is reported to be mainly mode I [22]. This means that the interlaminar fracture toughness values measured

from the mandrel peel test are expected to lie between the values measured by the DCB test (pure mode I) and the ELS test (pure mode II), though closer to DCB values than ELS ones.
The present work focuses on assessing the applicability of the mandrel peel test to quantify the fracture toughness of woven fabric based composites. A 5 Harness-Satin (HS) woven fabric carbon/PEEK laminate was chosen as a basis material. DCB and ELS test results were compared to mandrel peel test results for the same material system. Two directions of crack propagation were investigated. In the first case, the crack propagates parallel to the predominant fibre direction at the interface, while in the second case the crack propagates perpendicular to the predominant fibre direction. Finally, a microscopy analysis was performed to study the fracture surfaces of the different samples. The fractographic features observed in the test coupons were compared in order to identify the dominant failure modes during the mandrel peel test.

2. Experimental methods

The present section describes the specimen preparation as well as the procedures followed to characterise the interlaminar fracture toughness.

2.1 Specimen preparation

The material used in this research was a CETEX® 5 HS woven carbon fabric reinforced PEEK powder coated semi-preg supplied by TenCate. The fabric comprises 3K T300JB carbon fibre bundles with an equal amount of bundles in the warp and weft direction. The resulting repetitive unit cell has a dimension of 7.5x 7.5 mm^2, as shown in Figure 2. The figure also illustrates that a satin weave structure has a predominant fibre direction on each side of the fabric. On one side, e.g. the top view in Figure 2, this predominant fibre direction corresponds to the warp bundles, while on the other side the predominant fibre direction corresponds to the weft bundle direction.

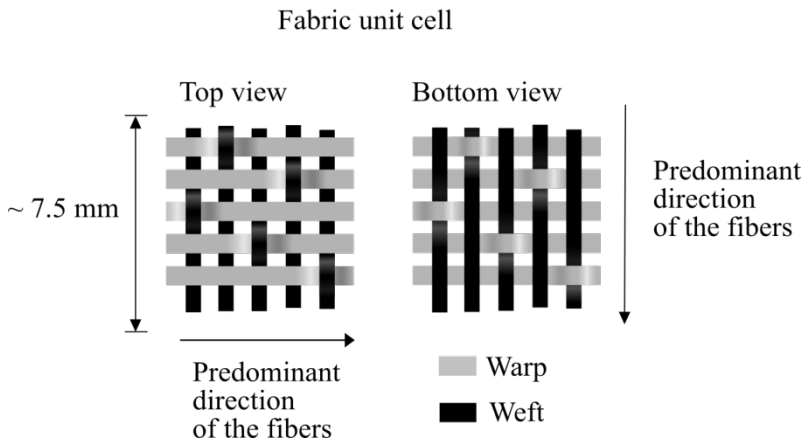

Figure 1: Schematic view of a unit cell for a 5 harness satin top and bottom view

A stacking sequence of $[(0/90)/(0/90)_r]_{4s}$ was used, in which r indicates a flipped or reversed ply, to prepare a single laminate from which all specimens were cut. As mentioned earlier two crack propagation directions were tested, parallel (//) and perpendicular (⊥)to the predominant fibre direction. Thus, two set of specimens were prepared for each one of the three testing techniques (DCB, ELS, and MP tests). All the test specimens required a pre-crack, which was in this case made by inserting a 13 μm thick Polyimide (PI) film (Upilex-S from UBE) during semi-preg stacking. The PI films were inserted in four locations as illustrated in Figure 3. The PI films were added at the midplane to obtain the ELS and DCB specimens, while the films were added between the first and second ply for the mandrel peel specimens. The laminate was subsequently press consolidated in a Pinette press at 10 bar and 380 °C, following the processing recommendations from the material supplier. Figure 4 shows the press cycle used to consolidate the laminate. A diamond-coated and water-cooled blade saw was used to cut the specimens from the laminate. Specimens of 20 mm width were cut for the DCB and ELS tests following the standards. The mandrel peel specimens were cut to a width of 10 mm, which is larger than the representative unit cell of the woven fabric.

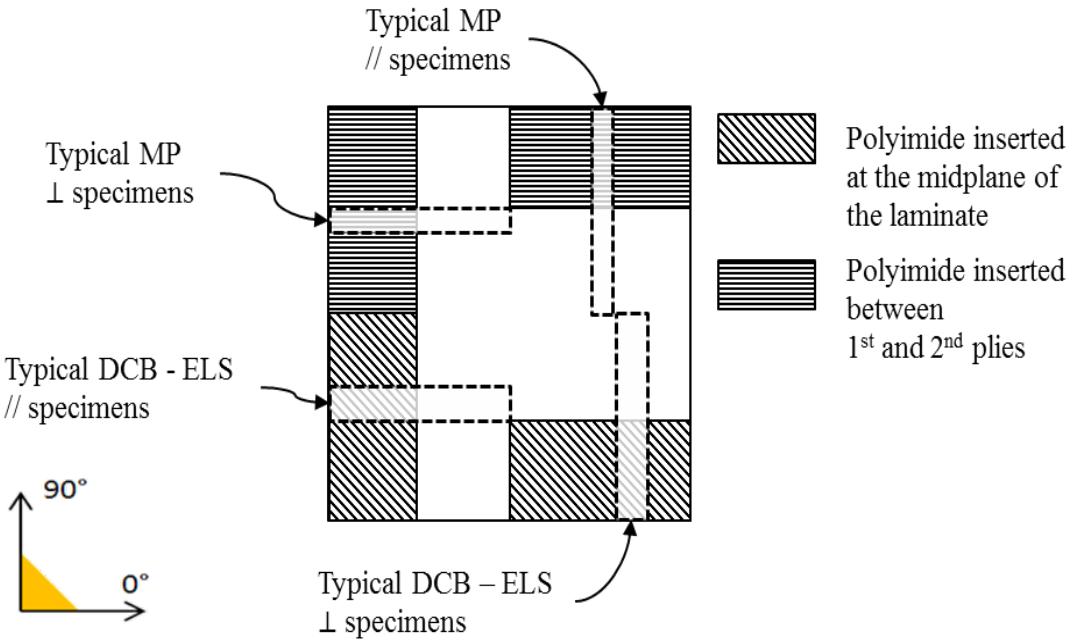

Figure 2: Schematic view of the position of the polyimide films placed before consolidation. The 0° corresponds to the Warp direction. MP: Mandrel Peel, DCB: Double Cantilever Beam, ELS: End-Loaded Split. //: Parallel. ⊥: Perpendicular.

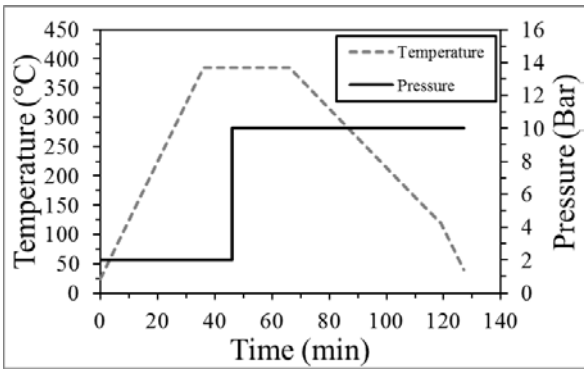

Figure 3: Schematic representation of the press consolidation cycle.

Figure 5 shows a schematic representation of the crack location for the different specimens. It can be seen that, technically, the mandrel peel interfaces are not exactly similar to the DCB and ELS interfaces when all the specimens are extracted from the same laminate. While the interface of DCB and ELS specimens predominantly comprises warp bundles, the interface of mandrel peel specimens predominantly comprises weft bundles. This choice was made in order to keep a symmetric layup. The authors believe, however, that this choice will have a negligible effect on the measured results, given the fact that the woven fabric is balanced in terms of properties according to the manufacturer technical data sheet [26]. Moreover, any influence of variations in processing conditions are prevented by extracting all specimens from the same laminate.

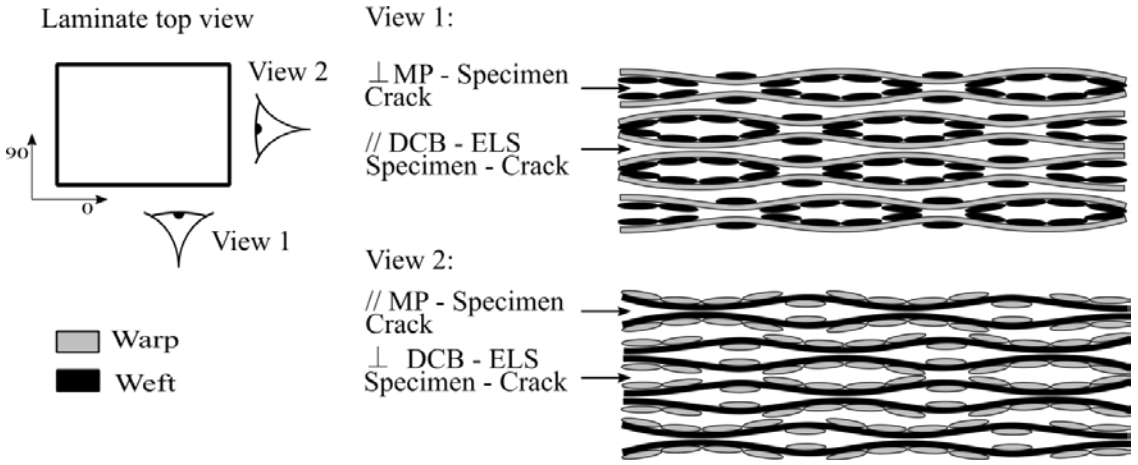

Figure 4: Schematic view of the stacking sequence and the position and direction of propagation of the crack. For the sake of clarity half of the plies are not shown. MP: Mandrel Peel, DCB: Double Cantilever Beam, ELS: End-Loaded Split. //: Parallel. ⊥: Perpendicular.

2.2 Double Cantilever Beam (DCB) test

The double cantilever beam tests were performed according to the ISO 15024 standard [27]. The Corrected Beam Theory (CBT) analysis was applied to calculate the mode I fracture toughness. According to this method, the critical energy release rate G_{IC} is given by:

$$G_{IC} = \frac{3P\delta}{2w(a+\Delta)}\left(\frac{F}{N}\right), \quad (1)$$

where w is the width of the specimen, P, δ and a are the force, displacement and crack length during crack propagation, respectively. Furthermore, F is a correction factor for the large displacement of the test specimen arms, N is a correction factor for the stiffening of the specimen by the load blocks and Δ is a correction for crack tip rotation and deflection.

The specimens were tested on a servohydraulic Instron 8500 universal testing machine, at a displacement rate of 1.2 mm/min. The testing machine was equipped with a HBM 200 N force cell and a 150 mm built-in Linear Variable Displacement Transducer (LVDT). The crack length was measured using an automated camera system engineered to follow the crack tip during the test using image recognition techniques. The camera was fitted with a 20x magnification lens. Since the delamination length was measured using the horizontal position of the travelling camera system, there is no need for a large-displacement correction factor, i.e. F can be considered equal to one [27]. The applied force P, the displacement δ, as well as the crack length a, were measured during the test. All DCB specimens showed unstable crack propagation. The first instability was not used to measure the fracture toughness, as the crack tip is affected by the manufacturing process and the crack initiation film. Unloading and reloading the specimens provided the initiation value, while the subsequent crack re-

initiations were used to calculate the propagation fracture toughness values.

2.3 End-Loaded Split (ELS) test

The end-loaded split test was performed according to the ISO 15114 standard [28]. The Instron 8500 servohydraulic universal testing machine mentioned earlier was fitted with a HBM 500 N force cell to perform the ELS test. Attempts to measure the crack length using the travelling camera system were unsuccessful, as it was difficult to identify the crack tip location accurately. Consequently, an apparent crack length was calculated from the compliance of the specimens following the procedure described in the standard ISO 15114 standard. According to this method, the compliance of the ELS specimen is expressed as:

$$C = \frac{\delta}{P} = \frac{(L + \Delta_{\text{clamp}})^3 + 3(a_{\text{app}})^3}{2wh^3E_1}, \tag{2}$$

where a_{app} is the apparent crack length, $E_1$is the apparent bending modulus, L is the span length, w is the width of the specimen and h half of the specimen thickness. The parameter $\Delta_{\text{clamp}}$was introduced by Hashemi [29] to consider the beam root deflection and rotations at the clamp point. The apparent crack length can be calculated from equation (2) at any moment of the test as:

$$a_{\text{app}} = \left(\frac{1}{3}\left\{2wCh^3E_1 - \left(L + \Delta_{\text{clamp}}\right)\right\}\right)^{\frac{1}{3}}. \tag{3}$$

The G_{IIC}values were determined using the Irwin-Kies equation:

$$G_{\text{IIC}} = \frac{P^2}{2w}\frac{\mathrm{d}C}{\mathrm{d}a}. \tag{4}$$

Substituting equation (2) into equation (4) yields:

$$G_{\text{IIC}} = \frac{9P^2(a_{\text{app}})^2}{4w^2h^3E_1}. \tag{5}$$

The parameters Δ_{clamp} and E_1 were measured according to the compliance calibration, also called ‘clamp correction’, described in the ISO 15114 standard.

Crack initiation was defined via the 5% criterion, i.e. by a 5% increase in initial compliance. For this purpose, the initial compliance C_0 was determined from a linear fit of initial force vs. displacement curve. The number of points used was such that the fit had an R^2 equal to 0.999. Following the standard, a new line was drawn with a compliance equal to $1.05C_0$. The intersection of this new line with the load-displacement curve yields the initiation load and displacement. During ELS testing all the specimens showed stable crack propagation.

Initiation and propagation values of fracture toughness were calculated. No pre-crack procedure was performed for the ELS specimens.

2.4 Mandrel Peel (MP) test

The mandrel peel setup is schematically represented in Figure 6. The setup used in this work had a mandrel with a radius of 10 mm. A constant displacement rate was applied using a Zwick universal testing machine on which the peel setup was mounted. The alignment force F_{a} necessary to conform the peel arm to the mandrel was applied using a pneumatic actuator.

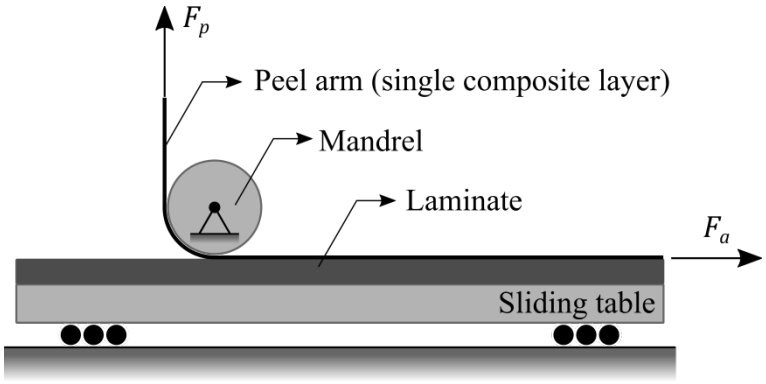

Figure 5: Schematic view of the mandrel peel test.

The effect of the alignment force [25], sample width and test speed [30] were investigated in previous research. No significant influence of these parameters on the test results was observed in the range of alignment force, sample width, and displacement speed tested. Following the result of the previously mentioned research, a constant peel rate of 30 mm/min and alignment force of 60 N were used in this work. Two HBM 200 N load cells were used to measure the alignment force F_{a} and peel force F_{p}. The critical energy rate can be calculated from the measured forces using Equation (6) [25],

$$G_{\mathrm{c}} = \frac{1}{w}(F_{\mathrm{p}}(1-\mu) - F_{\mathrm{a}}), \tag{6}$$

in which μ represents the friction coefficient in the setup. The test consists of two steps. First, the top ply is peeled from the laminate while measuring the peel force and the alignment force. Secondly, the cross head of the testing machine is returned to the initial position, and the test is performed again on the now de-bonded specimen (i.e. G_c is equal to zero), where the peel force and the alignment force are measured again. The friction coefficient can be obtained from this second step as:

$$\mu = \frac{F_p - F_a}{F_p} \tag{7}$$

An average friction coefficient (μ) value was calculated per each specimen. Subsequently an average friction coefficient was calculated for each sample as the mean of the specimen friction coefficients. Once the sample friction coefficient was calculated, the fracture toughness of the specimens can be calculated using the friction coefficient of the sample and equation (6). Four specimens were tested for each sample. All mandrel peel test samples showed unstable crack propagation. As with the DCB test, the first instability was not taken into account in the analysis. Only the subsequent crack re-initiations were used to calculate the fracture toughness values. The G_{IC} values for DCB and mandrel peel test are not referred as stable crack propagation values as the values are unstable crack propagation.

It is worth noting that the peel arm of the mandrel peel specimens showed a certain curvature before testing as shown schematically in Figure 7. The curvature of the peel arm is caused by process-induced residual thermal stresses present in the non-symmetric peel arm (which is a single 5HS woven fabric reinforced PEEK ply). These residual thermal stresses are released during crack propagation and need to be taken into account for accurate fracture toughness measurements [31]. Nevertheless, the contribution of the residual stresses to the interlaminar fracture toughness was estimated to be 1% for an interlaminar fracture toughness of 1 kJ/m^2. As such the residual stress were neglected in this research. The derivation of this estimation can be found in appendix A.

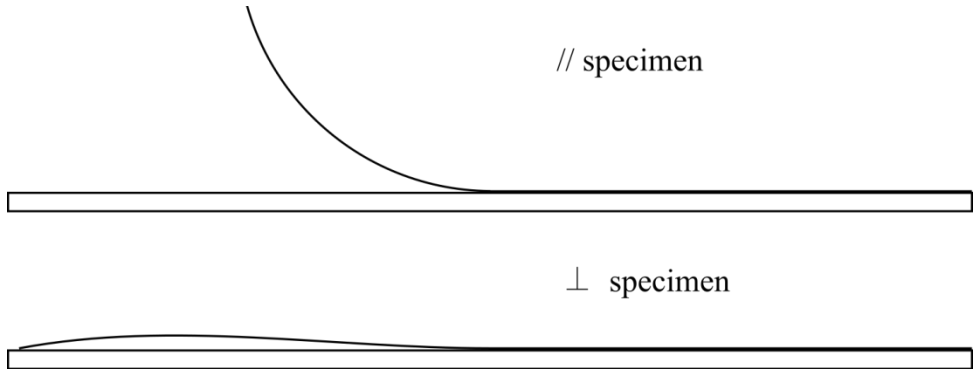

Figure 6 Schematic view of the mandrel peel specimens showing a typical curvature of the peel arm before testing. //: Parallel. ⊥: Perpendicular.

3. Results

The results of the different mechanical tests are presented in this section. Typical examples of force-displacement curves and R-curves (toughness vs. crack length) are shown for all the tests. The measured interlaminar fracture toughness values for the two types of samples (i.e. propagation parallel and perpendicular to the predominant fibre orientation) are presented. Finally, the results of the fractographic analysis of the different samples are described.

3.1 Double cantilever beam experiments

A typical force-displacement curve measured during the DCB test is shown in the left graph in Figure 8. A linear force vs. displacement behaviour can be observed during the initial loading phase until the crack suddenly initiates. This is accompanied by an abrupt and significant drop in force. The remainder of the test shows a similar repeated behaviour with a linear loading phase, followed by a sudden drop in force due to crack propagation. On average, such unstable crack propagation (stick-slip) is observed 5 to 6 times per specimen, corresponding to a total crack length of about 100 mm. The values of force, displacement, and crack length just before the unstable crack propagation were used to calculate the G_{IC}. The average crack propagation (or slip) distance for each instability was about 20 mm for the parallel specimens (i.e. crack propagation parallel to the predominant fibre orientation) and 16 mm for the perpendicular specimens (i.e. crack propagation perpendicular to the predominant fibre orientation). The linear force vs. displacement traces allows the use of linear elastic fracture mechanics. It is worth adding in this context that no significant permanent deformations of the specimens was observed after unloading. Nevertheless, the validity of analysis by energy release rate is questionable as no stable crack propagation was observed.

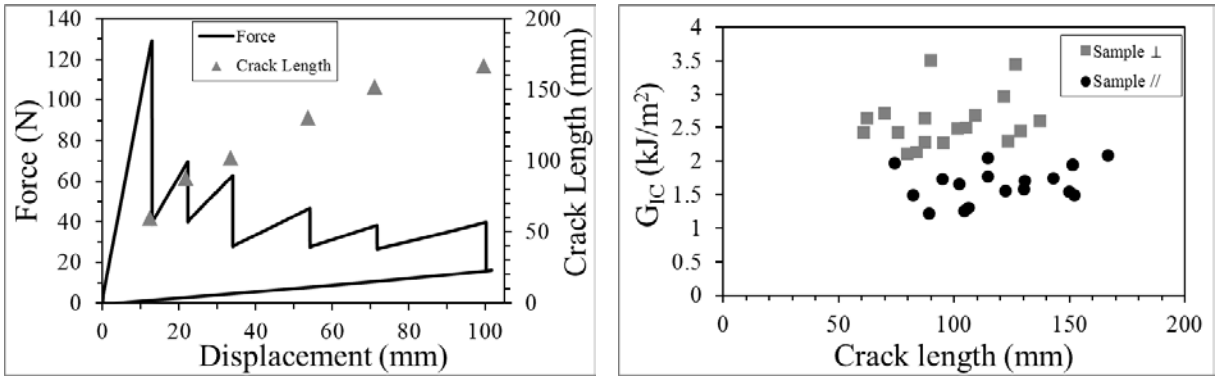

Figure 7: Left) The black line shows a typical force-displacement curve for a DCB test (// specimen). The grey triangles represent the crack lengths just before the unstable crack propagation starts. Right) Fracture toughness vs. crack length for all the DCB specimens. //: Parallel. ⊥: Perpendicular.

The right graph in Figure 8 shows the resistance points (fracture toughness) versus crack length produced by all specimens. Even though the scatter of the values is quite large, it can be observed that the R-curves for both samples can be considered as flat. The average values and standard deviations were calculated for each specimen. The average value for a single specimen was then used to calculate the average G_{IC} value of the sample and its standard deviation. The results of the DCB tests on a specimen level and sample level are shown in

Figure 9. It can be seen that both the fracture toughness of the perpendicular ⊥ specimens and sample exceeds that of the parallel // specimens and sample.

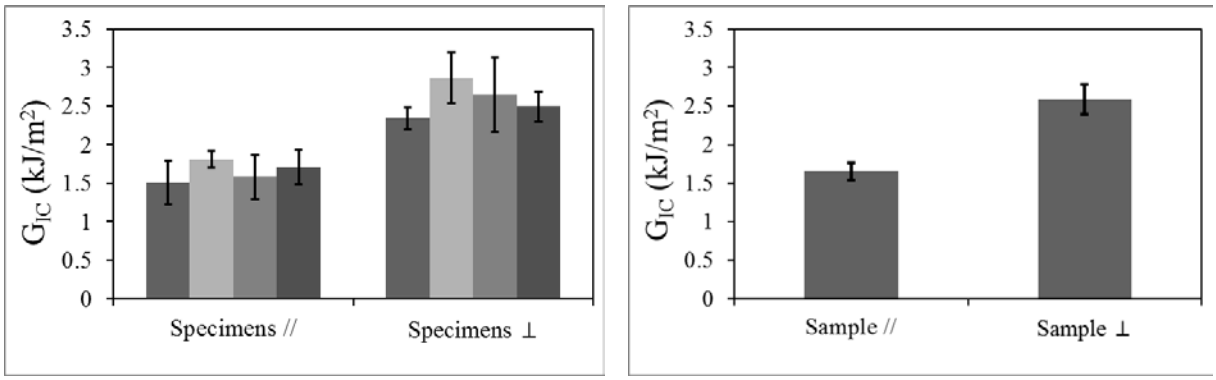

Figure 8: Left) Average toughness values for the different specimens with standard deviation. Right) Average toughness values for the different samples with standard deviation

3.2 End-loaded split experiments

According to the procedure outlined in the standard, a compliance calibration test was performed prior to the ELS test. The resulting values for the apparent bending modulus E_1 as well as the correction factor Δ, required to calculate the fracture toughness, can be found in Table 1.

Sample	Modulus $\boldsymbol{E_1}$(GPa) Compliance calibration	Δ factor (mm) Compliance calibration
Parallel (//)	55	5.5
Perpendicular (⊥)	52	7.2

Table 1: Results from the compliance calibration test.

Typical force-displacement curves measured during the ELS test for the parallel and perpendicular samples are shown in Figure 10 left. The force vs. displacement traces show a linear behaviour almost until the maximum force is reached. The star symbol in the left graph in Figure 10 represents the crack initiation point according to the 5% criterion, as described in the experimental section. Stable crack propagation was observed during the test, as can also be observed from the measurements of the apparent crack length. Finally, the left graph in Figure 10 indicates that the specimens showed slight residual deformation after testing, which can be caused by plastic deformation or damage (beside the measured delamination) during the test. The nonlinear loading stage and the residual displacement after unloading makes application of a LEFM approach somewhat questionable.

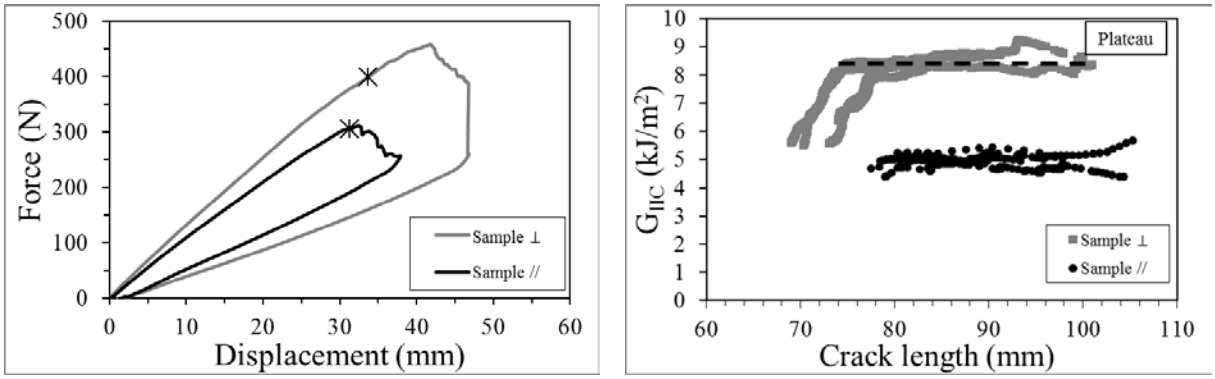

Figure 9: Left) Force vs. displacement curve. The star symbol represents the position of the crack initiation. Right) Fracture toughness vs crack length for all the specimens

The right graph in Figure 10 shows the R-curves for all the specimens. The curves with lower G_{IIC} values correspond to the specimens from the parallel sample, while the curves with a higher toughness correspond to the specimens from the perpendicular sample. The specimens from the parallel sample show a flat R-curve and the propagation values for this sample were calculated as an average G_{IIC} along the R-curve. The R-curves of the perpendicular specimens initially show an increasing trend until they level off to a plateau. This behaviour could be associated with the development of a damage zone in front of the crack tip as the crack starts to propagate [32] [33]. In the perpendicular specimens, the propagation values were calculated from the plateau region. The fracture toughness corresponding to crack initiation and crack propagation are shown in Figure 11. It can be seen that the initial fracture toughness of the perpendicular sample is slightly higher that of the parallel sample. Whereas, it can be seen that the propagation fracture toughness of the perpendicular ⊥ specimens exceeds that of the parallel // specimens.

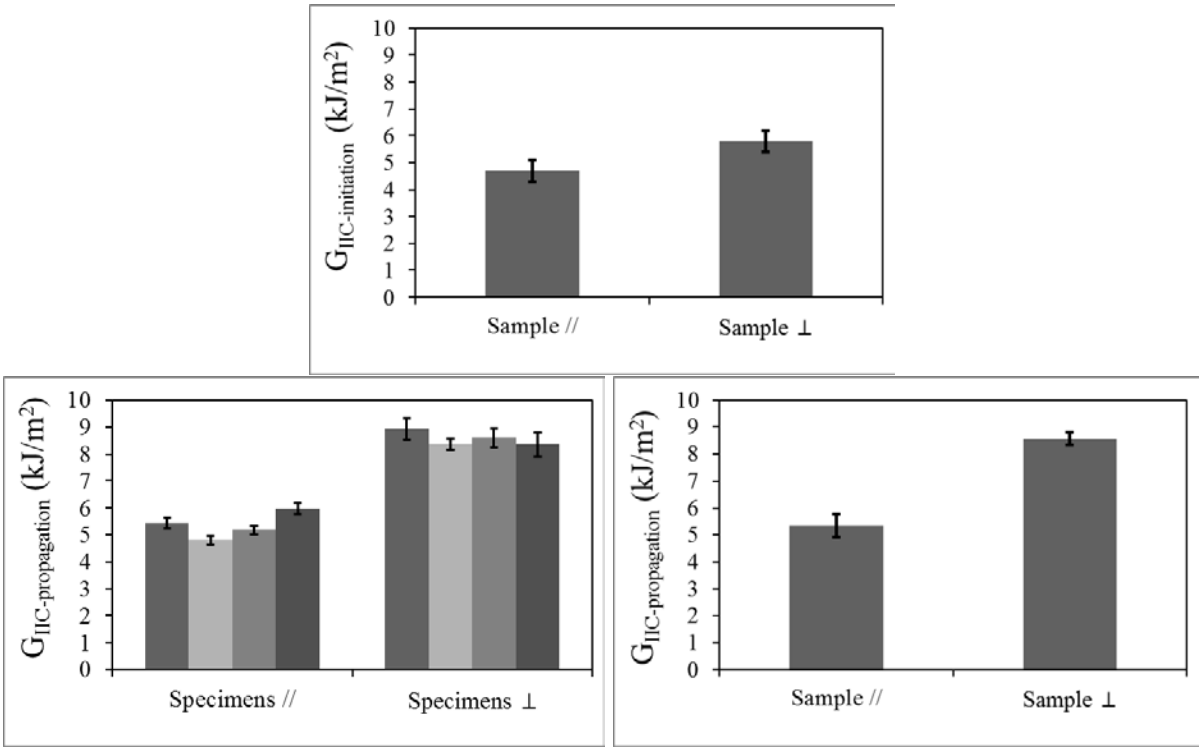

Figure 10: Upper)Initiation toughness values for the different samples with standard deviation. Bottom-left) Average propagation-toughness values for the different specimens with standard deviation. Bottom-right) Average propagation toughness values for the different samples with standard deviation.

3.3 Mandrel peel experiments.

The left graph in Figure 12 shows a typical force-displacement curve of a mandrel peel test for a parallel specimen and a force-displacement curve of the subsequent friction measurement. The friction coefficients for the parallel sample and perpendicular sample were 1.2±0.1% and 1.8±0.2%, respectively.

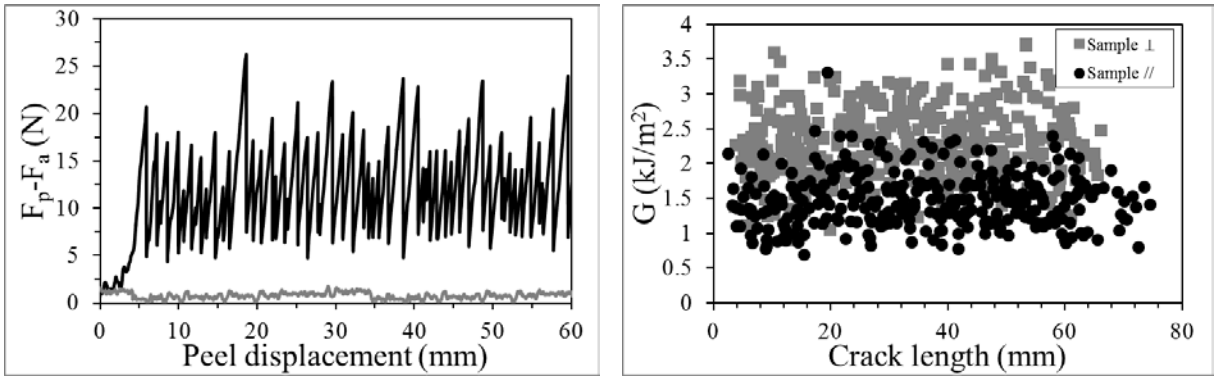

Figure 11 Left)Force vs. displacement during the mandrel peel test. The black line shows the actual test, while the grey line represents the subsequent run on the (now un-bonded) specimen to determine the friction in the setup. Right) Fracture toughness vs crack length for all the mandrel peel specimens

During the mandrel peel test, crack propagation showed a typical stick-slip behaviour. The repetitive behaviour of the test is schematically represented in Figure 13. At the beginning of

the loading phase, the peel arm conforms to the mandrel (stage A). As the loading increase, no crack propagation is observed (stick), and the conformation of the peel arm to the mandrel cannot be maintained (stage B). As the force increases and reaches a peak load, the stored energy in the system is enough to propagate the crack (stage C). A sudden unstable crack propagation is observed accompanied with an abrupt drop in the force (slip). By the end of this abrupt crack propagation, the peel arm completely conforms to the mandrel (stage A). This behaviour was repeatedly observed during testing.

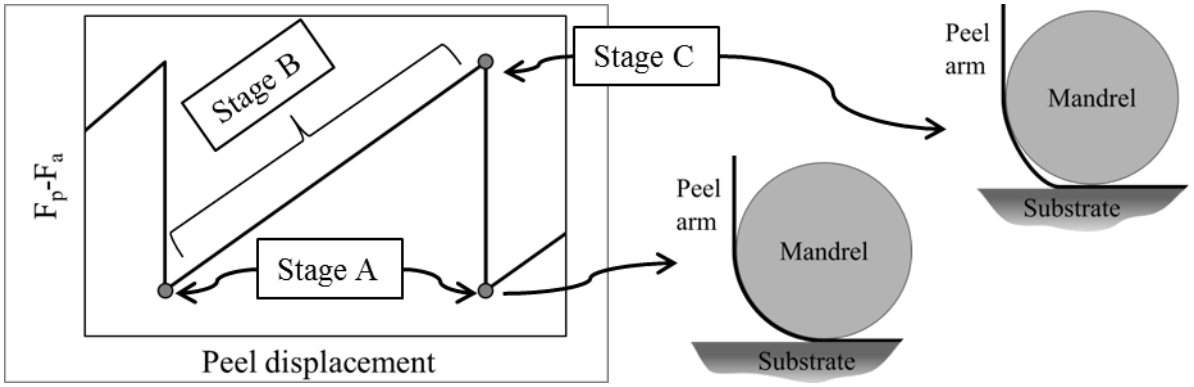

Figure 12: Schematic illustration of the of the peel arm behaviour during testing.

Similar to the DCB analysis, the peak values in the force-displacement graphs were used to calculate the toughness values. The right graph in Figure 12 shows the interlaminar fracture toughness as a function of the peel distance (R-curve) measured for all the specimens. Similarly to the DCB test results, the R-curve remains flat along the crack length although the spread in values is quite large.

The average interlaminar fracture toughness per specimen is shown in the left graph in Figure 14. Subsequently, one interlaminar fracture toughness value per sample was calculated using the specimen averages (see Figure 14 right). The variation per specimens is seen to be large, though the results are consistent within the sample. Also here, and similar to the DCB and ELS results, the perpendicular sample is shown to have a higher fracture toughness than the parallel sample.

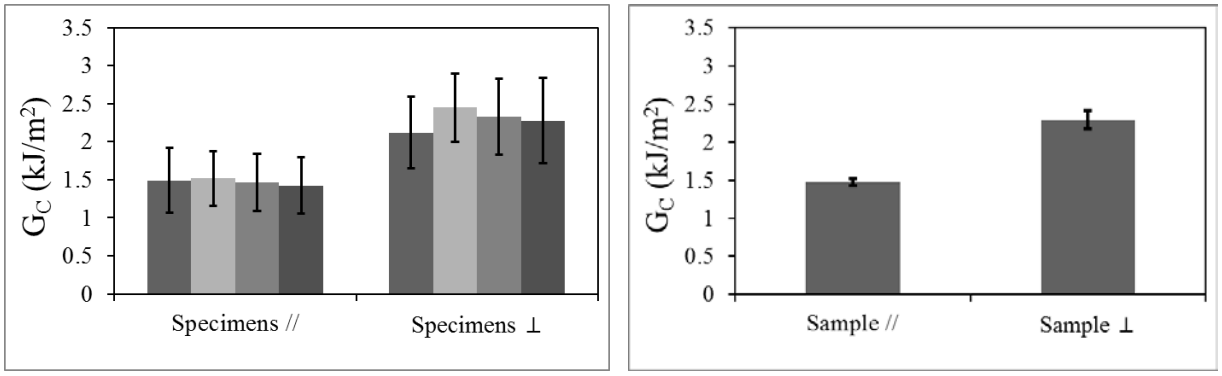

Figure 13: Left) Average toughness values for the different specimens with standard deviation. Right) Toughness values for the different samples with standard deviation.

3.4 Fractographic Analysis.

The fracture surfaces were analysed using optical microscopy and Scanning Electron Microscopy (SEM). Firstly, a comparison at a low magnification of the failure surfaces of a parallel and a perpendicular specimen is presented in order to identify the mechanisms that cause the higher toughness of the perpendicular samples. Secondly, an analysis at higher magnifications is presented, with the main objective of identifying the predominant failure modes (i.e. opening, shearing or mixed) during the MP test.

3.4.1 Influence of crack propagation direction

Figure 15 shows the fracture surfaces of a perpendicular (left) and parallel (right) DCB specimen, with the crack propagating from right to left. Both surfaces look quite similar and show fibre bundles as well as matrix rich regions between the bundles most of the times. Opposed to what is shown by other authors in similar testing [7] , [34], crack deflection and branching were rarely observed. The difference in toughness between the parallel and perpendicular samples can be explained by considering the interface morphology. Two factors will be elaborated here. The first is related to the constituents at the crack front, while the second is related to the crack path tortuosity.

The following analysis assumes that the crack front is a straight line, perpendicular to the crack propagation, which in practice is most probably not the case. Figure 16 provides a schematic representation of the fracture surfaces to ease the analysis regarding the first point. The left illustration shows that the crack front for the parallel specimens is composed of both fibre bundles and matrix pockets. Moreover, this composition does not change with crack propagation provided the crack is wide compared to the unit cell size. This is not the case for the perpendicular specimens, as is shown in the right illustration. Here, the constituent

composition at the crack tip varies along the crack length with matrix rich zones between the bundles exactly lining up with the crack front at regular intervals. At these instances the crack, across its full width, is forced to propagate through the tough matrix material, resulting in high load peaks and interlaminar toughness as was shown in the previous section.

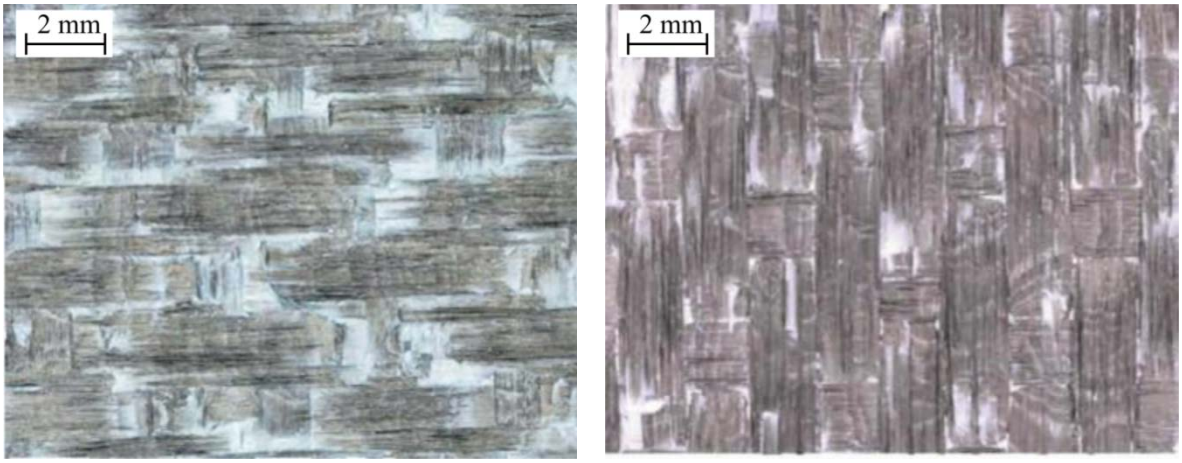

Figure 14: Fracture surface of two DCB specimens. Left) parallel specimens. Right) a perpendicular specimen. The crack propagation is from right to left

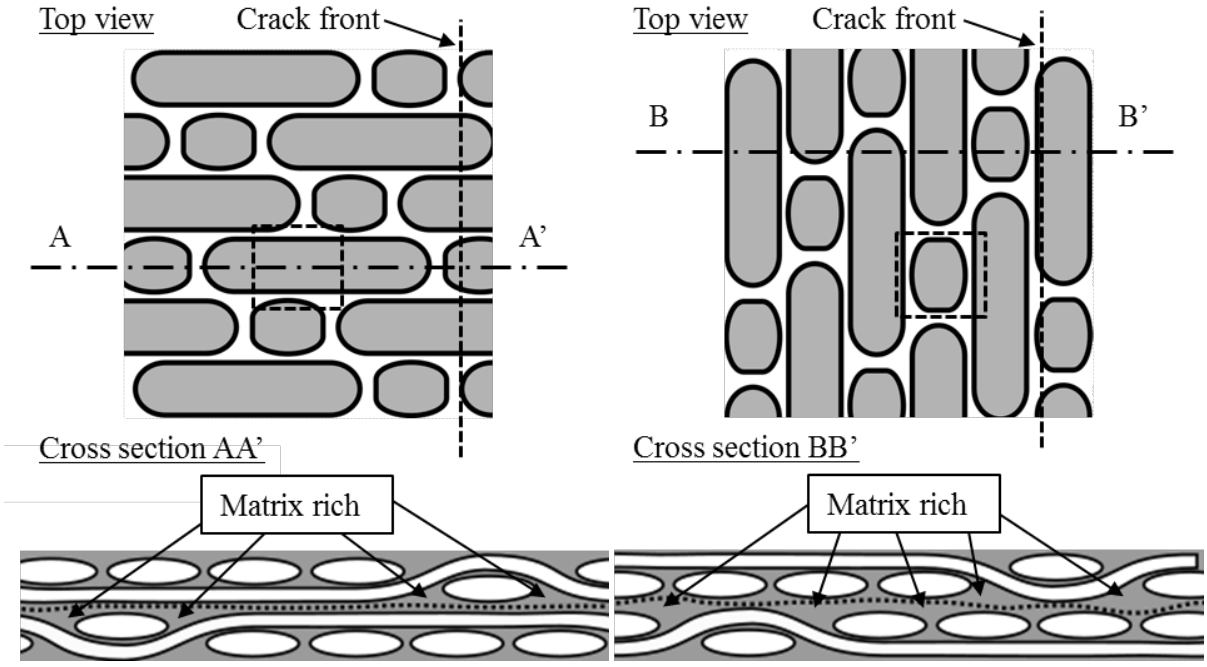

Figure 15: Left) Represent a parallel (//) specimen, Right) represent a perpendicular (⊥) specimen. The square boxes represent the areas where the high magnification SEM image was taken. The dotted lines in the bottom image (cross-section) represent the crack propagation path.

Apart from the constituent composition at the crack tip, the interlaminar toughness is also influenced by the tortuosity of the crack path with an increase in tortuosity leading to an

increase of interlaminar toughness [7]. To investigate whether this played a role here, the height profile (roughness) of the delaminated surfaces were characterized using a confocal microscope. Figure 17 shows the obtained images for both specimen types. The crack path shows a higher tortuosity in case the crack propagation direction is perpendicular to the predominant fibre direction, i.e. the right graph in Figure 17. Similar observations were made by other authors as well [3], [34], [7]. As mentioned earlier, the higher tortuosity is reported to result in a higher interlaminar toughness.

Both factors, i.e. the alignment of matrix rich zones with the crack front and the high crack path tortuosity, are believed to contribute to the increased interlaminar toughness of the perpendicular samples.

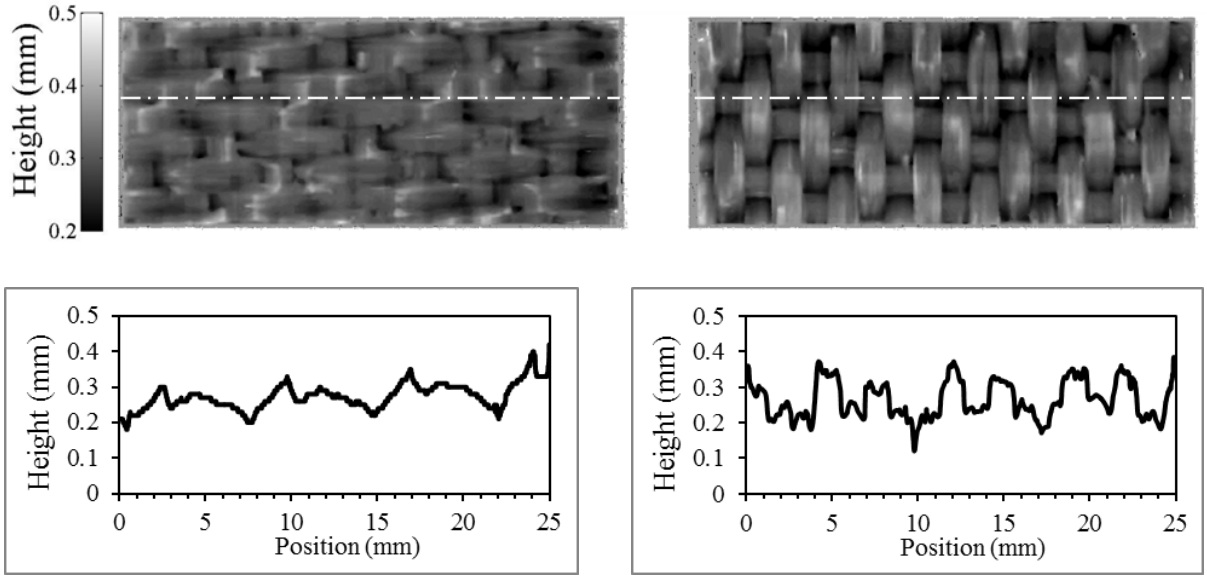

Figure 16: Fracture surface topology. Left) a DCB parallel specimen. Right) a DCB perpendicular specimen. The white dash-dotted line represents the position where the height was analysed in the lower charts.

3.4.2 Mandrel peel failure mode

The fracture surfaces of the DCB and ELS samples were also analysed to identify the characteristic features of pure mode I and pure mode II failure and compare these to that of the mandrel peel specimens. Figure 18, Figure 19 and Figure 20 show the fracture surfaces of the parallel specimens tested using DCB, ELS and mandrel peel, respectively. The area where the micrographs were taken is schematically represented in Figure 16. Figure 18 shows the fracture surface of a DCB specimen. Two regions can be distinguished. The main and predominant region corresponds to fast brittle failure characterised by rivers, scarps and cusps (Figure 18 left and centre) [35]. The second region is characterised by a larger amount of plastic deformation and drawing of the matrix, which is related to slow ductile plastic

deformation [35]. The latter features were difficult to find. They appear as narrow strips close to the positions where unstable crack propagation starts.

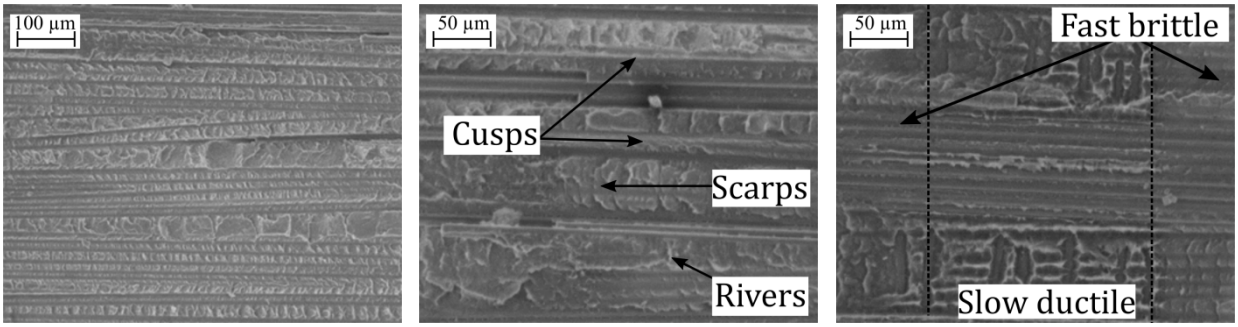

Figure 17: SEM fractography of a // DCB specimen. The image corresponds to a bundle with the fibres oriented in the same direction of the crack propagation. The crack propagates from right to left. Left) Region of unstable crack propagation. Centre) A zoomed-in look at a region of unstable crack propagation. Right) A zoomed-in look at a stable crack propagation region.

The fracture surface of the ELS specimen in Figure 19 shows traces of significant shear deformation of the matrix material. The drawing direction of the matrix material is in the same plane as the fracture surface. These failure features are typical for mode II failure [36].

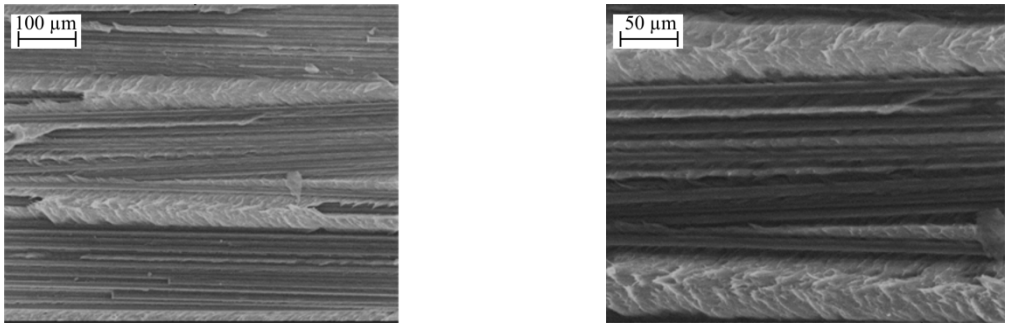

Figure 18 SEM fractography of a // ELS specimen where the crack propagates from right to left. The right image is a detail and close-up view of the left image

Finally, the fracture surfaces of a MP specimen are shown in Figure 20. The same two regions observed in the DCB sample, related to fast brittle propagation and to slow ductile failure, can also be found here. In this case, however, the regions corresponding to slow crack propagation are easier to find than in the DCB specimens, and apparent large plastic deformation of the matrix is observed. Nevertheless, the unstable crack propagation region is also still predominantly observed in the fracture surface. The features related to mode II failure were not observed in the mandrel peel specimens. This suggests that the failure mode of the mandrel peel test specimens was mainly an opening failure mode.

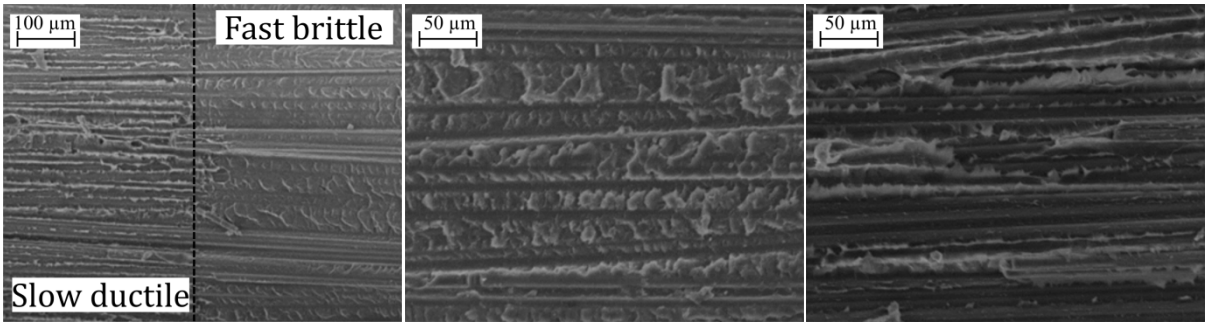

Figure 19: SEM fractography of a mandrel peel specimen. The crack propagates from right to left. Left) combination ofstable and unstable crack propagation. Centre) closer look at the region of unstable crack propagation. Right) Closer look at a region of stable crack propagation.

4. Discussion

The applicability and validity of the mandrel peel test for the characterization and measurement of interlaminar fracture toughness of woven composites based on the presented results is discussed here. The interlaminar fracture toughness values as measured using the DCB, ELS and mandrel peel test methods are summarised in Table 2. As it can be seen, the fracture toughness values measured by the mandrel peel test are close to the values obtained by DCB testing and far from the ELS test results. Moreover the characteristic features of opening mode failure shown by the fracture surfaces of the mandrel peel specimens further reinforce the idea that the mode mixity of the mandrel peel test is low and it is close to mode I. For this reason, the MP test is only compared with DCB tests in the remainder of this section. Further, the discussion concentrates on the test methodology and does not address the difference between parallel and perpendicular direction which was already elaborated in the results section

Sample	DCB (kJ/m^2)	MP test (kJ/m^2)	ELS Initiation (kJ/m^2)	ELS Propagation (kJ/m^2)
Parallel (//)	1.65±0.12	1.50±0.08	4.7±0.4	5.3±0.4
Perpendicular (⊥)	2.59±0.19	2.29±0.12	5.8±0.4	8.5±0.2

Table 2: Mean sample interlaminar fracture toughness values measured by DCB, MP, and ELS test with one standard deviation.

From a practical viewpoint, the mandrel peel test was found to be relatively simple to perform with straightforward simple sample preparation and data reduction procedure. The mandrel peel test requires less instrumentation compared to the DCB test, as there is no need to measure the crack length during testing. Moreover, at least for the material system tested in this work, the mandrel peel test generates more fracture toughness values for a single specimen than the DCB test. This is due to the mandrel which arrests any unstable crack

propagation. The distance between subsequent instabilities, calculated as the average incremental crack growth length between two maximum force peaks, is shown in Table 3. It can be noticed that the incremental crack growth length for the mandrel peel test is more than 20 times shorter distance than the value observed in the DCB test. Consequently, for specimens of the same length the mandrel peel test generates more data points that DCB test resulting in a higher statistical relevance of the results of the mandrel peel test. Moreover the table also illustrates that the average incremental crack growth length between subsequent instabilities is shorter for the perpendicular sample than for the parallel sample. This may suggest that crack arresting point is also governed by the woven structure, the thoughness of the specimen and the mandrel peel set up, therefore, further research is required to understand the governing mechanism behind this observation.

Sample	average incremental crack growth length (mm)	Standard deviation (mm)
DCB //	20.3	2.2
DCB⊥	16.9	2.0
MP //	0.83	0.07
MP⊥	0.48	0.05

Table 3: Average distance between peaks for the different samples tested

Figure 21 shows the average fracture toughness and standard deviation measured by DCB and mandrel peel test for each specimen (left) and the sample (right). For both samples, parallel and perpendicular, it can be observed that the DCB and MP tests yield a similar interlaminar fracture toughness value. Nevertheless, at specimen level (left graph in Figure 22), the DCB test shows slightly lower standard deviation compared to mandrel peel test, although the number of points per test is rather limited (<10). Furthermore, at sample and specimen level, the DCB shows a slightly higher mean value compared to the mandrel peel test, which will be addressed hereafter. The possible reason for this observation is discussed hereafter.

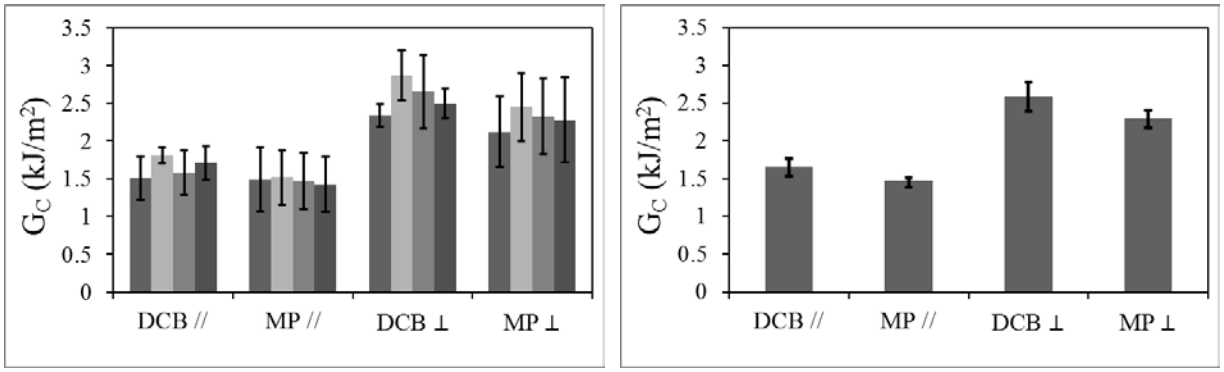

Figure 20: Left) Average Toughness values for the different specimens with standard deviation. Right) Toughness values for the different samples with standard deviation.

Figure 22 shows a plot of normalized frequency of the interlaminar fracture toughness for the two test methods. All single interlaminar fracture toughness values measured for each specimen within each sample were considered as independent values to calculate the frequency of occurrence. A normal distribution fit was used to interpret the results. Firstly, it can be noted that the MP test follows a normal distribution fit, whereas the DCB results do not follow the normal distribution as well as the mandrel peel results. This could partly be due to the lower number of values within the population of the DCB test samples. Secondly, a slight difference in the mean values between the DCB and the mandrel peel can be noticed, where the DCB test shows higher interlaminar fracture toughness for both parallel and perpendicular samples. Finally, it can be noted that, for both tests, the tails of the normal distributions for high values overlap, while the lower tail of MP test extends to smaller values as well. From a physical viewpoint, the difference in mean value and the position of the normal distribution tails can be explained as follows. During DCB testing, each time unstable crack propagation occurs, the material itself has to stop the instability. Therefore, the probability of crack arrest is higher in the tougher (matrix rich) regions. During the MP test, however, unstable crack propagation is mainly arrested by the mandrel, which means that the crack arrest position will not necessarily be in a region of high toughness. As discussed earlier, this is also shown by the average incremental crack growth length which does not correspond to typical average weave related distances. The subsequent re-initiation toughness values are measured close to the crack arrest points. Thus, the DCB test measures the fracture toughness in a tough region, while mandrel peel test measures the fracture toughness in more random position. These phenomenon might explains the observation that the DCB test measures a higher apparent toughness values as compared to the mandrel peel test. In other words, the tougher regions are over-represented in the DCB data, which results in an overestimation of the fracture toughness.

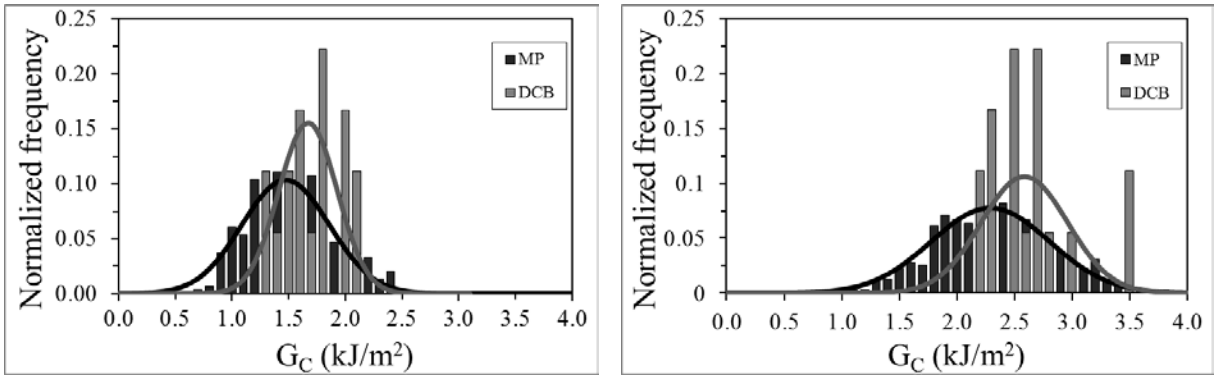

Figure 21: Normalized frequency in function of interlaminar fracture toughness for double cantilever beam (DCB) and mandrel peel test (MP). Left parallel sample . Right) Perpendicular sample.

Another possible factor that could contribute to the difference in the values measured between mandrel peel test and DCB test is that the interface for both tests is not exactly the same, as indicated earlier. In the DCB specimens, the crack propagates along the warp bundles, whereas it travels along the weft bundles for the mandrel peel specimens. The effect of crack travelling along warp or weft fibres on the interlaminar fracture toughness is not well described in the open literature, and therefore further attention is required in the future. Ideally, the mandrel peel test is performed on specimens having a pre-crack between the 2nd and the 3rd ply. This would ensure testing of the same interface for the three tests (DCB, ELS and mandrel peel test), while still being able to get the specimens from a single laminate. Moreover, this would also prevent the aforementioned peel arm deformation as a result of residual stresses. It is good to mention here that some specimens with such a configuration were tested. Unfortunately, a 2-ply peel arm was found to be too stiff to allow conformance to the roller without breakage. Still the effect crack traveling along warp or weft fibres on the interlaminar fracture toughness is not well described in the open literature, and therefore further attention is required in the future.

5. Conclusions

The interlaminar fracture toughness of a woven 5HS carbon/PEEK laminate was investigated using the Double Cantilever Beam (DCB), End-Loaded Split (ELS), and Mandrel Peel (MP) test methods. Crack propagation in two directions was studied, i.e. crack propagation parallel and perpendicular to the predominant fibre direction at the interface. As expected, the perpendicular samples showed a higher fracture toughness than the parallel ones. Furthermore, in line with observations from other researchers, the ELS test showed higher toughness than the DCB test. Also, both DCB and MP showed unstable crack propagation, whereas crack propagation was stable in ELS tests. The interlaminar fracture toughness

values measured by the mandrel peel test were similar to the values measured by the DCB test, which suggests that the mode-mixity of the mandrel peel test is low and hence it is close to mode I. Moreover, reinforcing this idea, the DCB and mandrel peel test specimens both show characteristic fractographic features of mode I failure, while ELS specimens show characteristic features of shear mode failure.

The mandrel peel test can be considered to be an easy and fast test compared to the DCB test. In this work, it was suggested that the presence of a strong stick-slip behaviour in the DCB test tends to overestimate the interlaminar fracture toughness values. Moreover, the mandrel peel test is able to measure the fracture toughness over a large number of distributed points in the test area, producing more than 20 times the amount of data points per unit crack length compared to the DCB test. The higher amount of crack (re-)initiation points measured by the mandrel peel test can be considered to make the mandrel peel test statistically more relevant than the DCB test. To conclude, the mandrel peel test seems to be an interesting alternative to the DCB test for woven fabric reinforced composites.

Acknowledgments

The authors gratefully acknowledge the financial as well as technical support from the industrial and academic members of the ThermoPlastic composites Research Centre (TPRC) as well as the support funding from the Province of Overijssel for improving the regional knowledge position within the Technology Base Twente initiative.

Appendix - A

The energy release per unit area associated with the thermal stresses was calculated from the curvature of the peel arm, as the change in elastic energy from the flat configuration to the curved configuration. Considering a beam subjected to a pure bending, the curvature (k) of its neutral line can be expressed as:

$$k = \frac{1}{\rho} = \frac{M}{EI}, \tag{8}$$

where ρ is the radius of curvature, M the moment applied to the beam, E the bending modulus, and I the moment of inertia. The strain energy of a beam subjected to a bending moment M is equal to

$$U = \frac{1}{2}\int_0^l \left(\frac{M^2}{EI}\right) dx\,. \tag{9}$$

Combining (8) and (9) the strain energy per unit of area can be calculated as

$$\frac{dU}{dA} = \frac{1}{2w}\frac{EI}{\rho^2} = \frac{1}{24}\frac{Eh^3}{\rho^2}, \tag{10}$$

where w is the width of the beam. The radius of curvature of the peel arm was measured by taking pictures of the un-bonded peel arm using an HP scanner at a resolution of 2400 DPI. The images were then analysed using the software package ImageJ. An approximate radius of curvature of 75 mm was measured for both parallel and perpendicular specimen, but in opposite directions. For simplification, the bending modulus of the peel arm was considered as the bending modulus measured in the compliance calibration test (see Table 1). The thickness of the peel arm was measured as 0.3 mm using a micrometre screw gage. A total energy per unit of area of around 10 J/m^2 was calculated using the aforementioned values. For this case it can be seen that the residual thermal stresses contribute less than 1 % to the total energy release rate compared with the interlaminar fracture toughness measured with the mandrel peel test. For this reason the residual stresses were neglected in this study.

References

[1] I. Paris, P. J. Minguet and K. T. O'Brien, "Comparison of delamination characterization for IM7/8552 composite woven and tape laminates," *ASTM STP 1436*, p. 372–390, 2003.

[2] P. Suppakul and S. Bandyopadhyay, "The effect of weave pattern on the mode-I interlaminar fracture energy of E-glass/vinyl ester composites," *Compos. Sci. Technol.*, vol. 62, p. 709–717, 2002.

[3] N. Alif, L. A. Carlsson and L. Boogh, "The effect of weave pattern and crack propagation direction on mode I delamination resistance of woven glass and carbon composites," *Composites Part B*, vol. 29, p. 603–611, 1998.

[4] M. Kotaki and H. Hamada, "Effect of interfacial properties and weave structure on mode I interlaminar fracture behaviour of glass satin woven fabric composites," *Composites Part A*, vol. 28A, p. 257–266, 1997.

[5] B. J. Briscoe, R. S. Court and D. R. Williams, "The effect of fabric weave and surface texture on the interlaminar fracture toughness of aramid/epoxy laminates," *Compos. Sci. Technol.*, vol. 47, p. 261–270, 1993.

[6] A. F. Gill, P. Robinson and S. Pinho, "Effect of variation in fibre volume fraction on modes I and II delamination behavior of 5HS woven composites manufactured by RTM," *Compos. Sci. Technol.*, vol. 69, p. 2368–2375, 2009.

[7] T. Ogasawara, A. Yoshimura, T. Ishikawa, R. Takahashi, N. Sasakib and T. Ogawa, "Interlaminar fracture toughness of 5 harness satin woven fabric carbon fiber/epoxy composites," *Advanced Composite Materials*, vol. 21.1, pp. 45-56, 2012.

[8] M. Olave, I. Vara, H. Husabiaga, L. Aretxabaleta, S. V. Lomov and D. Vandepitte, "Nesting effect on the mode I fracture toughness of woven laminates," *Composites Part A: Applied Science and Manufacturing*, vol. 74, pp. 166-173, 2015.

[9] T. K. O'Brien, "Interlaminar fracture toughness: the long and winding road to standardization.," *Composites- Part B: Engineering.*, vol. 29B(1), p. 57–62, 1998.

[10] A. J. Brunner, B. R. K. Blackman and P. Davies, "A status report on delamination resistance testing of polymer–matrix composites," *Engineering Fracture Mechanics*, vol. 75(9), pp. 2779-2794, 2008.

[11] I. Da Baere and et al., "Study of the Mode I and Mode II interlaminar behaviour of a carbon fabric reinforced thermoplastic.," *Polymer Testing*, vol. 31.2, pp. 322-332, 2012.

[12] R. Frassine and A. Pavan, "Viscoelastic effects on the interlaminar fracture behaviour of thermoplastic matrix composites: I. Rate and temperature dependence in unidirectional PEI/carbon-fibre laminates," *Composites Science and Technology,* vol. 54, 1995.

[13] R. Fracasso, M. Rink, A. Pavan and R. Frassine, "Effects of strain-rate and temperature on the interlaminar fracture toughness of interleaved PEEK/CF composites.," *Composites Science and Technology,* vol. 61(1), pp. 57-63, 2001.

[14] P. Compston and P. Jar, "Comparison of interlaminar fracture toughness in unidirectional and woven roving marine composites.," *Applied Composite Materials,* vol. 5.3, pp. 189-206, 1998.

[15] T. W. Webb and E. C. Aifantis, "Crack growth resistance curves and stick-slip fracture inestabilities," *Mechanics Research Communications,* vol. 24, pp. 123-130, 1997.

[16] T. W. Webb and E. C. Aifantis, "Stick- Slip Instabilities in Fracture," *Computational Mechanics,* pp. 1353-1358, 1995.

[17] D. Barquins and M. Maugis, "Stick-Slip and peeling of adhesive tapes," *Adhesion,* vol. 12, p. 205–222, 1988.

[18] M. Ciccotia, B. Giorgini and M. Barquins, "Stick-slip in the peeling of an adhesive tape: evolution of theoretical model," *International Journal of Adhesion and Adhesives,* vol. 18, no. 1, pp. 35-40, 1998.

[19] A. J. Kinloch, C. C. Lau and J. G. Williams, "The peeling of flexible laminates," *International Journal of Fracture,* vol. 66, pp. 45-70, 1994.

[20] P. J. Hine, B. Brew, R. A. Duckett and I. M. Ward, "Failure mechanisms in continuous carbon-fibre reinforced PEEK composites.," *Compos. Sci. Technol.,* vol. 35, pp. 31-51, 1989.

[21] "ISO 8510-1:1990 stadnad. Adhesives - Peel test for a flexible-bonded-to-rigid test specimen assembly - Part 1: 90 degree peel," 1990.

[22] L. F. Kawashita, D. R. Moore and J. G. Williams, "The Development of a Mandrel Peel Test for the Measurement of Adhesive Fracture Toughness of Epoxy–Metal Laminates," *The Journal of Adhesion,* vol. 80 (3), p. 147–167, 2004.

[23] T. Kok, W. J. Grouve, L. L. Warnet and R. Akkerman, "Effect of ply orientation on bond strength in fiber-placed composites," *ICCM20 proceedings.,* 2015.

[24] Y. Su, M. de Rooija, W. J. Grouve and L. L. Warnet, "Characterisation of metal-thermoplastic composite hybrid joints by means of a mandrel peel test," *Composites Part B: Engineering,* vol. 95, pp. 293-300, 2016.

[25] W. J. Grouve, L. L. Warnet and R. Akkerman, "Critical assessment of the mandrel peel test for fiber reinforced thermoplastic laminates," *Eng. Frac. Mech,* vol. 101, p. 96–108, 2013.

[26] "TenCate material, datasheets," 2017. [Online]. Available: http://www.tencate.com/advancedcomposites/default.aspx.

[27] "ISO 15024 Standard Test Method for Mode I interlaminar Fracture Toughness, Gic, of unidirectional Fibre-Reinforced Polymer Matrix Composites," 1997.

[28] "ISO 15114- Fibre-reinforced plastic composites - Determination of the mode II fracture resistance for unidirectionally reinforced materials using the calibrated end-loaded split (C-ELS) test and an effective crack length approach," *International Organisation for Standardisation,* 2014.

[29] S. Hashemi, A. J. Kinloch and J. G. Williams, "The analysis of interlaminar fracture in uniaxial fibre-polymer composites.," *Proceedings of the Royal Society of London A: Mathematical, Physical and Engineering Sciences.,* vol. 427, 1990.

[30] F. Sacchetti, W. J. Grouve, L. L. Warnet and I. Fernandez Villegas, "Woven fabric composites: Can we peel it?. Procedia Structural Integrity," *Procedia Structural Integrity,* 2016.

[31] J. A. Nairn, "Fracture mechanics of composites with residual thermal stresses," *Journal of Applied Mechanics,* vol. 64.4, pp. 804-810, 1997.

[32] H. Vu-Khanh and H. Wang, "Use of end-loaded-split (ELS) test to study stable fracture behaviour of composites under mode II loading.," *Composite Structures,* Vols. 36(1-2), p. 71–79, 1996.

[33] S. Hashemi, A. J. Kinloch and J. G. Williams, "The effect of geometry, rate and temperature on the mode I, mode II and mixed-mode I/II interlaminar fracture of carbon-fiber/poly(ether-ether ketone) composites," *Journal of Composite Materials,* vol. 24, p. 918–956, 1990.

[34] N. Alif, L. A. Carlsson and J. W. Gillespie, "Mode I, mode II, and mixed mode interlaminar fracture of woven fabric carbon/epoxy," *Composite Materials: Testing and Design,* vol. 13, 1997.

[35] D. Purslow, "Matrix fractography of fibre-reinforced thermoplastics, Part 1. Peel failures.," *Composites,*

vol. 18.5, pp. 365-374, 1987.

[36] D. Purslow, "Matrix fractography of fibre-reinforced thermoplastics, Part 2. Shear failures," *Composites*, vol. 19.2, pp. 115-126, 1988.